ELSEVIER

Colloids and Surfaces
A: Physicochemical and Engineering Aspects 156 (1999) 137–144

COLLOIDS AND SURFACES A

www.elsevier.nl/locate/colsurfa

Equilibrium configurations of liquid droplets on solid surfaces under the influence of thin-film forces Part I. Thermodynamics

E.K. Yeh [1], John Newman, C.J. Radke *

Department of Chemical Engineering, University of California, Berkeley, CA 94720-1462, USA

Received 8 September 1998; accepted 18 January 1999

Abstract

We present a rigorous thermodynamic analysis of single-component, two-dimensional (cylindrical) and three-dimensional (axisymmetric) drops and bubbles on an ideal solid substrate when the drop or bubble is subject to thin-film forces. Minimization of the system isothermal Helmholtz free energy yields the classic augmented Young-Laplace differential equation describing droplet shape. Attendant boundary conditions emerge naturally including a new augmented Young relation when the solid surface is bare or a smooth transition to a uniform film encircling the droplet. Both adsorbed and wetting films are considered, depending on the detailed behavior of the disjoining-pressure isotherm. © 1999 Elsevier Science B.V. All rights reserved.

Keywords: Adsorbed and wetting films; Augmented Young–Laplace equation; Augmented Young equation; Bare and film-covered surfaces; Microcontact angles, Thin-film forces

1. Introduction

When a droplet or bubble immersed in a second immiscible fluid contacts a solid surface, a thin film of the discontinuous fluid can form near the three-phase contact line at separation distances from the solid of less than about 100 nm [1–7]. Such thin films originate from surface excess forces that on a per-unit-area basis are referred to as disjoining pressures, Π [1,2]. The variation of Π with separation distance, h, from the solid substrate is the disjoining-pressure isotherm and can be locally attractive (conjoining forces) or repulsive (disjoining forces) or both. Thin-film forces are also expressed in the language of a potential interaction energy, P, whose negative derivative with respect to film thickness specifies the disjoining pressure: $\Pi = -\mathrm{d}P/\mathrm{d}h$.

Early in the discovery of thin films, it was recognized that the forces underlying their existence influenced the shapes of droplets and bubbles residing on solid surfaces near their

* Corresponding author. Tel.: +1-510-6425204; fax: +1-510-6424778.

E-mail address: radke@cchem.berkely.edu (C.J. Radke)

[1] Present address: VLSI Technology, Inc., 1109 McKay Drive M/S 02, San Jose, CA 95131, USA.

0927-7757/99/$ - see front matter
PII: S0927-7757(99)00065-5

periphery. Indeed, by 1940 both Frumkin [8] and Deryagin [9,10] introduced an augmented Young–Laplace equation to account for these thin-film forces and utilized that result to establish a now well-known formula for the macroscopic contact angle, θ_E, of drops or bubbles on solid surfaces surrounded by a continuous thin film [11,12]:

$$\cos\theta_E = 1 + \frac{1}{\sigma}\int_0^{\Pi_f} h(\Pi')\,d\Pi' \qquad (1)$$

where σ is the bulk liquid/gas surface tension and the subscript f denotes the thin film.

More recently de Gennes [13] and Brochard-Wyart et al. [14] considered in more detail the shapes of droplets in the case of dry or bare surfaces where the solid does not permit adsorption from the gas phase. They introduced the spreading coefficient as an additional parameter and sketched various droplet shapes for Hamaker thin-film forces, both attractive and repulsive. These workers noted the existence of pancake shapes, although Ruckenstein and Lee apparently established such shapes somewhat earlier [15].

With few exceptions [16–18], little attention is paid to the thermodynamic basis for the modeling efforts on the role of thin-film forces on wettability and contact angles. In this study we present a thermodynamic analysis for a single-component drop or bubble immersed in its own continuous phase and perched on an ideal solid surface. Thin-film forces are present close to the solid surface, as expressed in terms of the $\Pi(h)$ or $P(h)$ isotherms. Both bare solid surfaces and those that are covered by wetting or adsorbed films are considered. Our effort resembles that of Marmur [17]. However, as a useful approximation, we adopt the classical viewpoint that all deviations from constant-curvature shapes near the solid wall are due to thin-film forces [9,10] and not to variations in the interfacial tensions near the three-phase contact line [19]. A second companion effort illustrates how the augmented Young–Laplace and augmented Young equations may be rationally analyzed and numerically evaluated to yield a wide and fascinating variety of droplet and bubble shapes, depending on the specifics of the thin-film forces [12].

2. Thermodynamics of cylindrical drops

Consider a single-component liquid drop on a smooth solid surface and in equilibrium with its own vapor, as illustrated in Fig. 1. The solid surface is inert, smooth, homogeneous and non-deformable, and gravity is neglected. We assume that the liquid may adsorb onto the solid surface from the vapor phase, thus changing the surface energy of the substrate. Later, we also consider a subcase where no vapor adsorbs so that the solid surrounding the liquid remains bare. The configuration of a bubble on the solid and immersed in its own condensate arises naturally as a part of our analysis and need not be considered separately. The system in Fig. 1 is otherwise enclosed in a rigid box by non-interacting walls that act as boundaries. In addition to bulk and interfacial energies, thin-film forces exist and become important near the periphery of the droplet, as specified by the interaction potential per unit area, P, describing the thin liquid film separating the liquid–gas and solid–liquid interfaces. Thermal equilibrium is imposed, and the total mass and volume of the fluid component are conserved along with the total surface area of the solid. Thus, to establish the equilibrium configuration of the droplet, we minimize the system Helmholtz free energy A. For a cylindrical or two-dimensional drop[2], we have that:

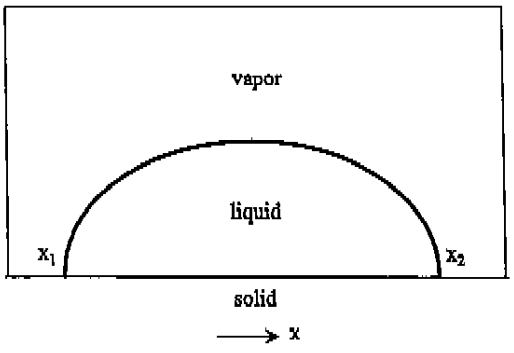

Fig. 1. The isothermal, closed thermodynamic system under consideration. Enclosed in the box is a liquid droplet atop a solid surface and surrounded by vapor.

[2] A two-dimensional drop exists in the x–z plane and is translationally invariant in the y-dimension. An axisymmetric or three-dimensional drop, considered later, is symmetric about the z-axis.

$$A = -p_L V_L - p_G V_G + \sigma_{SL} A_{SL} + \sigma_{SG} A_{SG} + \sigma A_{LG} + \mu_L n_L + \mu_G n_G + \mu_{SL} n_{SL} + \mu_{SG} n_{SG} + w \int_{x_1}^{x_2} P(h,h_x^2,h_{xx},\ldots)\,dx \quad (2)$$

For a macroscopic or large drop that partially extends beyond the range of thin-film forces, bulk liquid is present, and p_L is the corresponding bulk liquid pressure. However, for a microscopic or small drop which resides entirely within the range of thin-film forces, p_L remains a scalar constant, but it no longer corresponds to a bulk isotropic pressure. p_G is the gas pressure, and V_L and V_G are the volumes of the liquid and gas phases, respectively. A_{SL}, A_{SG} and A_{LG} are the areas of the solid–liquid, solid–gas and liquid–gas interfaces, respectively, while σ_{SL} and σ_{SG} denote the surface energies of the solid–liquid and solid–gas interfaces. σ is the surface tension of the liquid–gas interface. μ_L and μ_G are the chemical potentials of the liquid and vapor phases, respectively, and n_L and n_G are their corresponding mole numbers. n_{SL} and n_{SG} represent the Gibbs surface excess amounts adsorbed on the solid–vapor and solid–liquid surfaces [20], respectively, and μ_{SL} and μ_{SG} are their respective chemical potentials. Accordingly, the solid–gas surface energy depends on the pressure of the enveloping gas phase. No term appears for adsorption at the liquid–gas surface, as the Gibbs adsorption is zero for this interface [20].

w is a unit of width for the two-dimensional drop, and x_1 and x_2 are the x-coordinates of the edges of the drop where the liquid–vapor surface of the drop meets a bare surface. If the droplet terminates at a film, x_1 and x_2 constitute the box dimensions. Films may be of two types. Adsorbed films reflect finite vapor adsorption beyond the drop edges. Typically, for finite contact angles, adsorbed films are up to several monolayers in thickness [21,22]. Conversely, wetting films are generally much thicker [22]. Whether or not the solid–vapor interface is bare or is covered by an adsorbed or wetting film depends on the behavior of the thin-film forces, as discussed later. Drop height or thickness varies with x and is defined here by:

$$h(x) = \frac{1}{\rho_L} \int_0^{\infty} [\rho(x,z) - \rho_G]\,dz \qquad x_1 \le x \le x_2 \quad (3)$$

where $\rho(x,z)$ denotes the local fluid molar density profile extending from the solid surface into the vapor in the z-direction, and ρ_L and ρ_G are the bulk liquid and gas molar densities. $P(h,h_x^2,h_{xx},\ldots)$ in Eq. (2) is the thin-film potential energy of interaction between the liquid–vapor and solid–liquid interfaces, where the subscripts on drop thickness indicate differentiation. Here we note that P and the disjoining pressure Π may, in general, depend on film thickness, slope, curvature, and possibly higher order derivatives. In this work P specifically refers to a liquid-like film between the solid and the gas phases. In cases where, for example, a thin film circumscribes a necked droplet (i. e. $\theta_E > \pi/2$), so that vapor exists between the thin film and the droplet, our current analysis does not apply. All interfacial tensions in Eq. (2) refer to those far from the contact line. Hence, in our treatment, thin-film behavior at the droplet perimeter is reflected solely by the behavior of the $P(h,h_x^2,h_{xx},\ldots)$ isotherm.

We desire the equilibrium shape of the droplet, $h(x)$, which is specified by $dA = 0$ at constant temperature, mass, area and volume. Differentiation of Eq. (2) gives:

$$dA = -p_L\,dV_L - V_L\,dp_L - p_G\,dV_G - V_G\,dp_G + \sigma_{SL}\,dA_{SL} + A_{SL}\,d\sigma_{SL} + \sigma_{SG}\,dA_{SG} + A_{SG}\,d\sigma_{SG} + \sigma\,dA_{LG} + A_{LG}\,d\sigma + \mu_L\,dn_L + n_L\,d\mu_L + \mu_G\,dn_G + n_G\,d\mu_G + \mu_{SL}\,dn_{SL} + n_{SL}\,d\mu_{SL} + \mu_{SG}\,dn_{SG} + n_{SG}\,d\mu_{SG} + w\,d\int_{x_1}^{x_2} P(h,h_x^2,h_{xx},\ldots)\,dx = 0 \quad (4)$$

At constant temperature, the Gibbs–Duhem equations can be written for the bulk liquid and vapor phases:

$$-V_L\,dp_L + n_L\,d\mu_L = 0 \quad (5)$$

and

$$-V_G\,dp_G + n_G\,d\mu_G = 0 \quad (6)$$

Likewise, variations of the solid–vapor and solid–liquid interfacial energies are described by the isothermal Gibbs adsorption equations [20]:

$$A_{SL}\,d\sigma_{SL} + n_{SL}\,d\mu_{SL} = 0 \tag{7}$$

$$A_{SG}\,d\sigma_{SG} + n_{SG}\,d\mu_{SG} = 0 \tag{8}$$

and

$$d\sigma = 0 \tag{9}$$

This last expression indicates that, except at very large curvatures, there can be no change in the isothermal tension of the liquid–vapor interface [20].

Next, we invoke the constraints of constant mass, area and volume:

$$dn_L + dn_G + dn_{SL} + dn_{SG} = 0 \tag{10}$$

$$dA_{SL} + dA_{SG} = 0 \tag{11}$$

and

$$dV_L + dV_G = 0 \tag{12}$$

Substitution of Eqs. (5)–(12) into Eq. (4) yields the following important result:

$$\begin{aligned} dA = &-(p_L - p_G)\,dV_L + (\sigma_{SL} - \sigma_{SG})\,dA_{SL} \\ &+ \sigma\,dA_{LG} + (\mu_L - \mu_G)\,dn_L \\ &+ (\mu_{SL} - \mu_G)\,dn_{SL} + (\mu_{SG} - \mu_G)\,dn_{SG} \\ &+ w\,d\int_{x_1}^{x_2} P(h,h_x^2,h_{xx},\ldots)\,dx = 0 \end{aligned} \tag{13}$$

Note that the liquid molar density is not required to be constant, so that n_L and V_L are independent. Also in Eq. (13) it is recognized that n_L, n_{SL} and n_{SG} each vary independently of the remaining variables, and thus the coefficients of dn_L, dn_{SL} and dn_{SG} are identically zero. This result of equality of chemical potentials ($\mu_L = \mu_G = \mu_{SL} = \mu_{SG} = \mu$) signifies phase equilibrium. Variations in the remaining terms of Eq. (13) are interdependent. To clarify this interdependence we adopt the following geometric identities:

$$V_L = w\int_{x_1}^{x_2} h\,dx \tag{14}$$

$$A_{SL} = w\int_{x_1}^{x_2} dx \tag{15}$$

and

$$A_{LG} = ws = w\int_{x_1}^{x_2}\frac{ds}{dx}\,dx = w\int_{x_1}^{x_2}\sqrt{1+h_x^2}\,dx \tag{16}$$

where s in Eq. (16) is the arc length of the liquid–vapor interface and subscript notation is again used to signal a derivative. Eqs. (14)–(16) allow the remaining terms in Eq. (13) to be rewritten as:

$$d\int_0^{x_2}[\sigma\sqrt{1+h_x^2} + \sigma_{SL} - \sigma_{SG} + P + p_c h]\,dx = 0 \tag{17}$$

where, for convenience, symmetry of the drop shape is recognized, and where the pressure difference $p_G - p_L$ is identified as the capillary pressure p_c. In macroscopic systems, the capillary pressure is a well-defined and measurable quantity [23]. For microscopic droplets, however, p_c is a parameter that controls the drop size, with larger capillary pressures yielding smaller drops. The integral in Eq. (17) defines the appropriate free energy whose minimum characterizes the drop profile. Similar expressions have been put forward by de Gennes [13] and Brochard-Wyart et al. [14], but not in the context of a complete thermodynamic argument.

To establish the function $h(x)$ that minimizes the integral in Eq. (17) requires careful application of the calculus of variations [24]. As illustrated in Fig. 2, the non-standard feature of exploring the minimum of Eq. (17) is that the upper integral limit, x_2, changes as alternative drop profiles are explored. Let $h(x)$ in Eq. (17) be replaced by $h(x) = h(x) + \varepsilon\eta(x)$ where $h(x)$ is now the particular drop shape that satisfies Eq. (17). $\eta(x)$ is a continuously differentiable but otherwise arbitrary function, and ε is a constant parameter for each function $\eta(x)$. We use Leibnitz' rule [25] to differentiate Eq. (17) with respect to ε and evaluate the resulting expression at $\varepsilon = 0$ to give:

$$\begin{aligned} &\int_0^{x_2}\left[\frac{\sigma h_x}{\sqrt{1+h_x^2}}\frac{d\eta}{dx} + \frac{dP}{dh}\eta + p_c\eta\right]dx \\ &+ \frac{dx_2}{d\varepsilon}[\sigma\sqrt{1+h_x^2} + P(0) + \sigma_{SL} - \sigma_{SG}]_{x_2} = 0 \end{aligned} \tag{18}$$

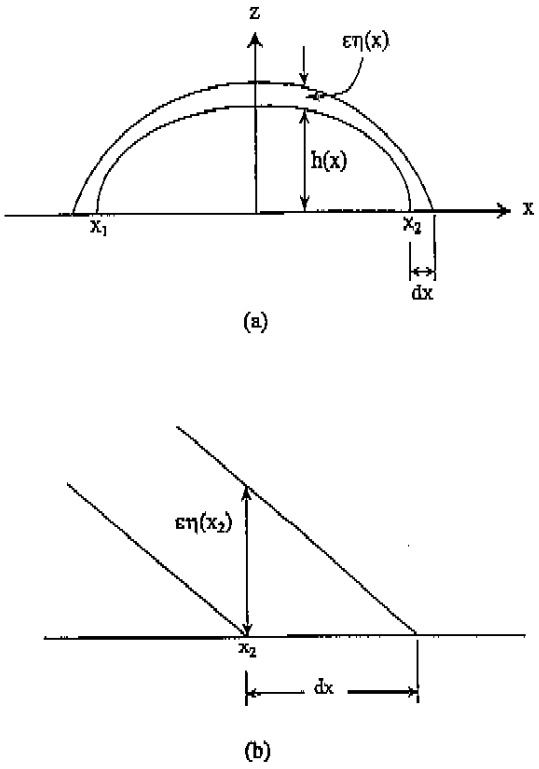

Fig. 2. (a) A two-dimensional drop of arbitrary shape, $h(x)$, on a bare solid surface. (b) The edge of the drop shown in part (a) and the basis of Eq. (19).

where we here specialize the thin-film forces to be functions only of h because little, if any, is known about the dependence of thin-film forces on higher order terms. From Fig. 2, $dx_2/d\varepsilon$ can be written as:

$$\frac{dx_2}{d\varepsilon} = -\eta(x_2)\frac{1}{h_x|_{x_2}} \tag{19}$$

Use of this result and integration by parts of the first term of the integrand in Eq. (18) gives the following result, after simplification:

$$\int_0^{x_2} \eta\left\{-\frac{\sigma h_{xx}}{[1+h_x^2]^{3/2}} + \frac{dP}{dh} + p_c\right\} dx - \eta\left\{\frac{1}{h_x}\left(\frac{\sigma}{\sqrt{1+h_x^2}} + P(0) + \sigma_{SL} - \sigma_{SG}\right)\right\}|_{x_2} = 0 \tag{20}$$

Note in this development that the droplet need not be of constant volume, as in other approaches [13,14,17]. Since η is an arbitrary function, each coefficient of η in Eq. (20) is independently equal to zero. The result is two conditions dictating the equilibrium configuration of a drop on a solid surface.

The first coefficient condition leads to the well-known augmented Young–Laplace equation in two dimensions [8–14]:

$$\frac{\sigma h_{xx}}{[1+h_x^2]^{3/2}} + \Pi(h) = p_c \tag{21}$$

where the first term reflects the transverse curvature of the droplet. Values of the capillary pressure set the basic equilibrium shapes. Positive values tend to yield bubbles, whereas negative values tend to yield droplets, although many more interesting shapes can arise, such as planar films, stepped films, pancakes, and wiggly bubbles and drops depending on the details of thin-film forces [12,26]. We refer generically to all of these shapes as droplets, unless specific cases are discussed. Also, small absolute values of p_c can produce macroscopic shapes that exhibit a constant-curvature portion with only their edges falling in the range of $P(h)$, whereas large absolute values of p_c produce microscopic shapes that lie entirely within the range of $P(h)$. If P depends on other variables than film thickness, then additional terms will appear in Eq. (21).

The second term multiplying η in Eq. (20) serves as a boundary condition for the augmented Young–Laplace equation:

$$\frac{\sigma}{\sqrt{1+h_x^2}} + P(0) + \sigma_{SL} - \sigma_{SG} = 0 \quad \text{at } h = 0 \tag{22}$$

where in this expression σ_{SG} corresponds to the bare-solid surface energy. To our knowledge this second condition has not been previously pointed out. Anywhere along the drop the local angle, θ, between the liquid–vapor surface and the plane of the solid is defined as $\theta = \tan^{-1}h_x$. Thus, Eq. (22) can be rewritten in the form:

$$\sigma\cos\theta_0 = \sigma_{SG} - \sigma_{SL} - P(0) \tag{23}$$

where θ_0 is the microscopic contact angle at the drop periphery [13–15]. The microscopic contact angle is to be distinguished from the macroscopic

contact angle, which exists only for macroscopic drops and is obtained by appropriate extrapolation from the droplet shape in the constant-curvature region [12]. Eq. (23) is analogous to the classical contact-line equilibrium constraint of Young [27], except that the influence of thin-film forces is now evident through the term $P(0) = \int_0^\infty \Pi(h)dh$. We call Eq. (23) the augmented Young relation. If we now define the spreading coefficient for a bare surface by $S = \sigma_{SG} - \sigma_{SL} - \sigma$, then the augmented Young equation reduces to:

$$\cos\theta_0 = 1 + \frac{S - P(0)}{\sigma} \quad \text{bare surface} \tag{24}$$

In the case of a bare surface, the spreading coefficient enters the problem as an independent parameter in addition to the behavior of the $P(h)$ isotherm. This expression proves useful as the boundary condition for quantitative calculation of droplet shapes resting on bare solids [12].

When, however, an adsorbed or wetting film encircles the droplet, x_1 and x_2 in Fig. 1 are fixed at the box edges, as a film of thickness h_f covers the remaining solid surface. In this case, the second term in Eq. (20) is not relevant. There is no corresponding augmented Young constraint at the droplet edge. The requisite boundary condition for solution of the augmented Young–Laplace equation is simply that the droplet meets the surrounding film smoothly or equivalently that h approaches h_f as $x \to \infty$. Interestingly, for film-covered solid surfaces, the spreading coefficient does not enter the problem.

Eq. (21) with its attendant boundary conditions at x_2 of Eq. (24) for a bare surface and an asymptotic approach to h_f for a film-covered surface provide the basis for numerical evaluation of cylindrical drop shapes given information on $P(h)$ and S [12].

3. Thermodynamics of axisymmetric drops

The Helmholtz free energy for axisymmetric droplets follows by analogy to the two-dimensional case. Thus, the thin-film-force term in Eq. (2) is replaced by $2\pi\int_0^{r_2} P(h) r\, dr$, where r is the radial coordinate for a drop of radius r_2 and where the interaction potential energy depends only on film thickness. The axisymmetric expressions for volume and area are now written as:

$$V_L = 2\pi \int_0^{r_2} hr\, dr \tag{25}$$

$$A_{SL} = 2\pi \int_0^{r_2} r\, dr \tag{26}$$

and

$$A_{LG} = 2\pi \int_0^{r_2} \frac{ds}{dr} r\, dr = 2\pi \int_0^{r_2} \sqrt{1 + h_r^2}\, r\, dr \tag{27}$$

Now by proceeding as above, we recover the expression for the pertinent free energy to be minimized:

$$d\int_0^{r_2} [\sigma\sqrt{1 + h_r^2} + \sigma_{SL} - \sigma_{SG} + P(h) - p_c h]\, r\, dr = 0 \tag{28}$$

Similar application of the calculus of variations leads to the axisymmetric form of Eq. (18):

$$\int_0^{r_2} \left[\frac{\sigma h_r}{\sqrt{1 + h_r^2}} \frac{d\eta}{dx} + \frac{dP}{dh}\eta + p_c\eta\right] r\, dr + r_2 \frac{dr_2}{d\varepsilon}[\sigma\sqrt{1 + h_r^2} - P(0) + \sigma_{SL} - \sigma_{SG}]_{r_2} = 0 \tag{29}$$

Since Eq. (19) still holds with r replacing x we find that:

$$\int_0^{r_2} \eta \left\{ - \frac{\sigma h_{rr}}{[1 + h_r^2]^{3/2}} - \frac{\sigma h_r}{r[1 + h_r^2]^{1/2}} + \frac{dP}{dh} + p_c \right\} r\, dr - r\eta \left\{ \frac{1}{h_r} \left(\frac{\sigma}{\sqrt{1 + h_r^2}} + P(0) + \sigma_{SL} - \sigma_{SG} \right) \right\} \Big|_{r_2} = 0 \tag{30}$$

which is the companion result to Eq. (20). Again, since each bracketed term in Eq. (30) is independent, the axisymmetric form of the augmented Young–Laplace equation is:

$$\sigma \left\{ \frac{h_{rr}}{[1 + h_r^2]^{3/2}} + \frac{h_r}{r[1 + h_r^2]^{1/2}} \right\} + \Pi(h) = p_c \tag{31}$$

where the additional term, as compared to the two-dimensional form, accounts for the circumferential curvature of the axisymmetric drop. The constraints at the droplet edge r_2 remain identical

to those for cylindrical drops, but now in radial coordinates. Thus, the analysis of axisymmetric drops parallels that of cylindrical drops [12].

The governing differential equations for both cylindrical and axisymmetric droplets are non-linear and require numerical solution. Details of the numerical procedures are available in the thesis of Yeh [26]. Numerous cases are presented and discussed by Yeh et al. [12].

4. Adsorbed versus wetting films

We refer above to the possibilities that droplets may be surrounded by adsorbed or wetting films. Which case arises depends primarily on the behavior of the $\Pi(h)$ isotherm. It is well known that planar thin films are unstable when $d\Pi/d(h) > 0$ [28]. Thus, thin planar films are possible when the value of the capillary pressure intersects the disjoining pressure curve at a point of local negative slope. Such films may surround droplets or cover the entire solid surface when no droplet is present.

Whether such a thin film is adsorbed or wetting now depends on the behavior of the disjoining-pressure isotherm and the value of p_c. For adsorption from the gas phase, adsorption isotherms, or $\Gamma_{SG} = n_{SG}/A_{SG}$ as a function of gas pressure, may be converted into disjoining-pressure isotherms, or Π as a function of adsorbed film thickness $h_f = \Gamma_{SG}/\rho_L$, by the following identity [11,29]:

$$\Pi = -\rho_L kT \ln\left(\frac{p_G}{p_{sat}}\right) \tag{32}$$

where k is Boltzmann's constant, T is the absolute temperature, and p_{sat} is the fluid vapor pressure. Thus, adsorption-isotherm expressions that describe the submonolayer to several monolayers regime can be converted into $\Pi(h)$ and $P(h)$ isotherms to characterize adsorbed films [29]. By way of example, for a simple fluid adsorbing on a solid surface Henry's law must emerge in the limit of vanishing gas pressure [30]:

$$\Gamma_{SG} = K_H p_G = \frac{h_f}{\rho_L} \quad p_G \to 0 \tag{33}$$

where K_H is Henry's constant for adsorption. Substitution of this result into Eq. (32) gives the functionality of the disjoining pressure for vanishingly small adsorbed film thicknesses:

$$\Pi = -\rho_L kT \ln\left(\frac{\rho_L}{K_H p_{sat}} h\right) \quad h \to 0 \tag{34}$$

where, for convenience, we have dropped the subscript denoting film on the adsorbed- layer thickness. Note that as h approaches zero, the disjoining pressure is logarithmically singular. Whenever the disjoining-pressure isotherm reflects the behavior of a gas adsorption isotherm so that it approaches infinity in the limit of zero thickness (i.e. zero adsorption), then adsorbed films are possible. Adsorbed films of molecular dimension arise when the capillary pressure intersects the disjoining-pressure isotherm in this regime. Conversely, wetting films are much thicker [21,22], and the corresponding form of the disjoining-pressure isotherm may be due to the more macroscopic descriptions of thin-film forces, such as that of Deryagin–Landau–Verwey–Overbeek theory [31]. However, if the disjoining-pressure isotherm terminates with a finite value at zero film thickness, then only a bare surface surrounding the droplet is possible when $p_c \geq \Pi(0)$.

An important point from Eq. (34) is that, although the disjoining pressure is infinite as thickness approaches zero, the corresponding interaction potential remains finite in this same limit:

$$P(h) = \rho_L kT\left[h \ln\left(\frac{\rho_L}{K_H p_{sat}} h\right) - h\right] + P(0) \quad h \to 0 \tag{35}$$

In this work, all interaction potentials terminate at zero thickness such that $P(0)$ is a finite constant.

The distinction between film-covered and bare solid surfaces is by definition. Bare surfaces permit no adsorption from the vapor phase. Monolayer or submonolayer gas-adsorption behavior appears in disjoining-pressure isotherms at thicknesses that are too thin to be resolved on the scale of nanometers. Hence, the bare-surface analysis for droplet and bubble shapes at much larger scales remains relevant.

5. Conclusions

Variational minimization of the Helmholtz free energy of a cylindrical (two-dimensional) or axisymmetric (three-dimensional) droplet on an ideal solid substrate whose edges fall under the influence of thin-film forces gives two conditions for the equilibrium shape. The first of these results is the familiar augmented Young–Laplace equation that specifies the equilibrium profile of the liquid–vapor surface. The second result serves as a boundary condition for the augmented Young–Laplace differential equation and depends on whether the solid substrate surrounding the droplet is bare or is covered by a thin film. For a bare solid substrate, an augmented Young equation arises specifying the microscopic contact angle at the edge of the drop. This new relation includes a term that accounts for the presence of the thin-film interaction potential, just as the augmented Young–Laplace is refined by the addition of a disjoining pressure. For a film-covered surface, adsorbed or wetting, the droplet must meet the film continuously and there is no separate augmented Young condition. The augmented Young–Laplace and its attendant Young and film-continuity boundary conditions provide the requisite tools for numerical calculation of a wide variety of droplet and/or bubble shapes given information on the thin-film forces and the spreading coefficient.

Acknowledgements

This work was partially supported by the US Department of Energy under Contract DE-AC03-76SF00098 with the Lawrence Berkeley National Laboratory of the University of California. Partial financial support for E.K.Y. was furnished by the Dow-Corning Corporation.

References

[1] B.V. Deryagin, M.M. Kussakov, Izv. Akad. Nauk SSSR Ser. Khim. 5 (1936) 741.
[2] B.V. Deryagin, M.M. Kussakov, Izv. Akad. Nauk SSSR Ser. Khim. 6 (1937) 1119.
[3] B.V. Deryagin, Z.M. Zorin, Zh. Fiz. Khim. 29 (1955) 1010.
[4] Z.M. Zorin, N.V. Charaev, Colloid J. 30 (1968) 279.
[5] T.D. Blake, J.A. Kitchener, J. Chem. Soc. Faraday Trans. 1 (1973) 1435.
[6] M.P. Aronson, M.F. Petko, H.M. Princen, J. Colloid Interface Sci. 65 (1978) 296.
[7] S. Basu, M.M. Sharma, J. Colloid Interface Sci. 181 (1996) 443.
[8] A.N. Frumkin, Zh. Fiz. Khim. 12 (1938) 337.
[9] B.V. Deryagin, Zh. Fiz. Khim. 14 (1940) 137.
[10] B.V. Deryagin, Kolloid Zh. 17 (1955) 207.
[11] N.V. Churaev, Rev. Phys. Appl. 23 (1988) 975.
[12] E.K. Yeh, J. Newman and C.J. Radke, Colloids Surf. A, 156 (1999) 137.
[13] P.M. de Gennes, Rev. Mod. Phys. 57 (1985) 827.
[14] F. Brochard-Wyart, J.M. di Meglio, D. Quéré, P.M. de Gennes, Langmuir 7 (1991) 335.
[15] E. Ruckenstein, P.S. Lee, Surface Sci. 52 (1975) 298.
[16] G.J. Hirasaki, in: N.R. Morrow (Ed.), Interfacial Phenomena in Petroleum Recovery, Marcel Dekker, New York, 1991 Chapter 2.
[17] A. Marmur, J. Colloid Interface Sci. 148 (1992) 541.
[18] E. Ruckenstein, J. Colloid Interface Sci. 179 (1996) 136.
[19] I.B. Ivanov, P.A. Kralchevsky, in: I.B. Ivanov Jr. (Ed.), Thin Liquid Films, Marcel Dekker, New York, 1988 Chapter 2.
[20] R. Defay, I. Prigogine, A. Bellemans, D.H. Everett, Surface Tension and Adsorption, Wiley, New York, 1966 Chapters I, II, VII.
[21] P. Huh, A.W. Adamson, J. Colloid Interface Sci. 59 (1977) 605.
[22] G.F. Teletzke, L.E. Scriven, H.T. Davis, J. Colloid Interface Sci. 87 (1982) 550.
[23] J.W. Amyx, D.M. Bass Jr., R.L. Whiting, Petroleum Reservoir Engineering, McGraw-Hill, New York, 1960 Chapter 3.
[24] M.D. Greenberg, Foundations of Applied Mathematics, Prentice-Hall, New York, 1978, pp. 202–209.
[25] F.B. Hildebrand, Advanced Calculus for Applications, 2nd ed., Prentice-Hall, New York, 1976, pp. 364–367.
[26] E.F. Yeh, M.S. Thesis, University of California, 1998.
[27] T. Young, Philos. Trans. R. Soc. London 95 (1805) 65.
[28] A. Vrij, Disc. Faraday Soc. 42 (1966) 23.
[29] G.J. Hirasaki, J. Adhesion Sci. Technol. 7 (1993) 285.
[30] J.A. Barker, D.H. Everett, Trans. Faraday Soc. 58 (1962) 1608.
[31] J.T.G. Overbeek, in: H.R. Kruyt (Ed.), Colloid Science, vol. 1, Elsevier, Amsterdam, 1952 Chapter VI.